Mechanism and Machine Theory 70 (2013) 266–277

Contents lists available at ScienceDirect

Mechanism and Machine Theory

journal homepage: www.elsevier.com/locate/mechmt

Robotic swimmer/pump based on an optimal wave generating mechanism

Eyal Setter, Izhak Bucher *

Faculty of Mechanical Engineering, Technion-Israel Inst. of Technology, Haifa 32000, Israel

ARTICLE INFO

Article history:
Received 28 August 2012
Received in revised form 21 July 2013
Accepted 23 July 2013
Available online xxxx

Keywords:
Cam-based mechanism
Traveling waves
Torque minimization
Fluid manipulation
Low Reynolds number environment

ABSTRACT

This paper describes a unique mechanism that generates longitudinally traveling waves as a means for fluid manipulation i.e., self-propulsion or pumping in low Reynolds number environments. Possible applications include small-scale micro-robotic swimmers or large-scale pumps for highly viscous fluids. The proposed mechanism generates axi-symmetrical transverse traveling waves along a cylindrical elastic membrane, and it is designed so that the required internal actuation torque on the input shaft is zero in the absence of friction. The paper also demonstrates that torque oscillations can be completely eliminated, even when motional friction exists and only a small constant torque is required to overcome friction. Since torque oscillations are associated with alternating stresses and fatigue, the proposed design increases the service life of the device and, moreover, considerably reduces the power consumption. It is demonstrated analytically and numerically that these properties are achieved by choosing a specific spatial rotational phase between successive cams, and by choosing a certain ratio between the number of wavelengths and cams along the device. A realistic macro-scale device that can be tuned to fulfil the optimal conditions is also described.

1. Introduction

Traveling mechanical waves are a physical phenomenon widely used in engineering and robotics. Vibration-induced traveling waves [1] are mainly used as a means for conveying objects, as in rotary or linear ultrasonic motors [2,3] or are coupled with acoustic levitation to reduce friction [4]. Low frequency traveling waves are encountered in self-propelled robots, such as snake-like robots moving on solid surfaces [5,6] and snail-like robots moving on a thin slime film [7]. Traveling waves as a means of self-propulsion in liquids are encountered in a large variety of Reynolds number environments. In high Reynolds number environments where inertia dominates viscous forces, waving fins are employed to propel biomimetic fish-like robots [8]. Under low Reynolds number conditions, as in small scales or highly viscous environments, the dynamics is governed mainly by viscous effects. Therefore, any transport mechanism must rely on non-inertial and non-time reversible trajectories [9]. These conditions are fully satisfied by traveling mechanical waves, one of the common motility mechanisms for unicellular creatures [10,11]. Traveling waves are also utilized in micro-robotic artificial swimmers [12], and more recently in micro pumps as well [13,14]. The growing interest in micro-swimmers stems from their potential therapeutic capabilities, such as targeted drug delivery and non-invasive micro surgery and diagnosis [15].

Vibration-induced traveling waves [16] are energetically advantageous when the device exploits natural resonance phenomena [17]. Yet, in the present case, resonance cannot be utilized due to incompatible time-scales and the relatively large required amplitudes [18], making it impractical and highly inefficient. Moreover, the hydrodynamic efficiencies of low Reynolds fluid manipulators are rather low [19]. Therefore, especially in small-scale autonomous mobile applications where weight and volume constraints are critical, an efficient propulsion mechanism is required.

* Corresponding author. Tel.: +972 48293153; fax: +972 48295711.
E-mail address: bucher@technion.ac.il (I. Bucher).

0094-114X/$ – see front matter © 2013 Elsevier Ltd. All rights reserved.
http://dx.doi.org/10.1016/j.mechmachtheory.2013.07.017

The paper describes an optimal mechanism that produces a traveling wave-like deformation sequence along a cylindrical elastic membrane, thus acting as a pump when positioned inside a tube or as a free swimmer in low Reynolds numbers. The special arrangement of the mechanism eliminates the internal torque oscillations or equivalent speed fluctuations. The mechanism uses multiple cams with several cam-followers per cam such that the total torque required by the driving motor is minimized. The elastic forces of the membrane and the inertia forces of the reciprocating cam-followers are shown to be completely balanced out and the only remaining effects are due to friction, which necessitates only a small constant motor torque to operate.

1.1. Swimming/pumping principle in brief

As mentioned above, traveling waves are a non-time-reversible sequence of shape deformation, which is thus applicable for low Reynolds number fluid manipulation, i.e. swimming or pumping. Similarly to the case of a waving 2D (two-dimensional) membrane [19,20], in the absence of inertia, the velocity of the solid particles experiencing a traveling wave create a vorticity field in the adjacent fluid, which is characterized by rotating vortices, in our case toroidal. These vortices induce a net flow in the direction of the wave propagation, in the case of a fixed pump, or inflict stresses that propel a free swimmer in a direction opposite to the wave direction of propagation, see Fig. 1. For a more detailed analytical model see Ref. [18].

In the subsequent sections the proposed model is presented, followed by an analytical analysis of the kinematics and dynamics. Next, a robotic prototype capable of realizing the proposed scheme is described. The paper closes with several conclusions.

2. Mechanism description and analysis

Consider a rotating cam driving a reciprocating cam-follower (roller type) while rotating at a constant speed Ω. The instantaneous contact points P_1 and P_2 shown in Fig. 2 dictate whether the motor should drive the rotating cam or be driven by it. It is thus understood that the applied torque, which yields constant angular velocity of the cam, is oscillating. In Section 2.2 it is demonstrated that the special arrangement of the multi-cam device eliminates the torque oscillations or equivalent speed fluctuations.

The mechanism's schematics are illustrated in Fig. 3. In this figure, a set of successive cams is positioned along a common input shaft to form a monolithic rigid camshaft. The cams, via cam-followers and arched beams, make the peripheral elastic cylindrical membrane deform in a desired sequence (Figs. 2–3). As the cams revolve, the cam-followers reciprocate radially, while the arched beams are kept in contact with the pre-tensioned exterior elastic cylindrical membrane. Thus, the cylindrical membrane deforms periodically in the desired traveling wave manner. All parts except for the surrounding elastic membrane are assumed rigid. The geometrical properties of the wave can be tuned by the cam profile and by the spatial angular phase between successive cams along the camshaft. The wave frequency is determined by the cam profile and by the shaft angular velocity Ω. As illustrated in Fig. 3, the number of cams, N_C, and the number of angular wavelengths per cam, N, are by nature integers. This, however, is not necessarily the case for the number of wavelengths along the mechanism M. The relation between these parameters and the cam profile is discussed in Section 2.2 with respect to minimizing the input torque by exploiting the restoring forces of the elastic membrane. The proposed mechanism was fabricated and recorded during operation (300 frames per second), as shown in Clip 1. The clip shows the deformation in time of the cylindrical membrane due to cam operation. The filmed configuration consists of

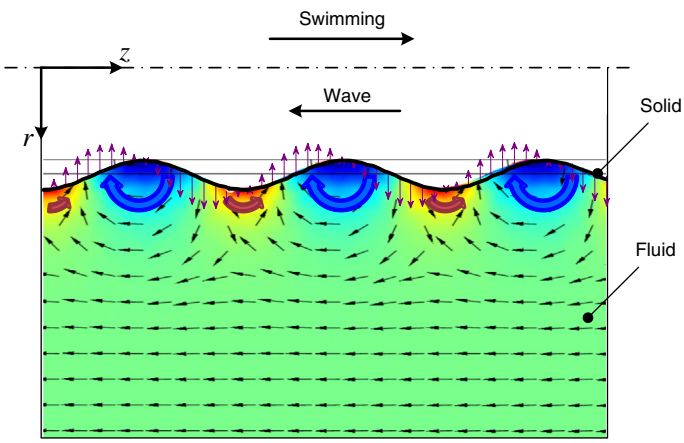

Fig. 1. Numerical simulation of the axi-symmetric vorticity field (color-coded) and normalized velocity field (black arrows) generated in a fluid adjacent to a waving axi-symmetric cylinder in low Reynolds number environment. The velocity of the waving solid particles (vertical purple arrows) induce vorticity of alternating signs (red and blue). The vorticity of greater magnitude and extent (blue surface) is generated in the sinusoid valleys and induces a net flow in the direction of the wave propagation in the case of a fixed pump, or stresses that propel a free swimmer in a direction opposite to the wave propagation. (For interpretation of the references to color in this figure legend, the reader is referred to the web version of this article.)

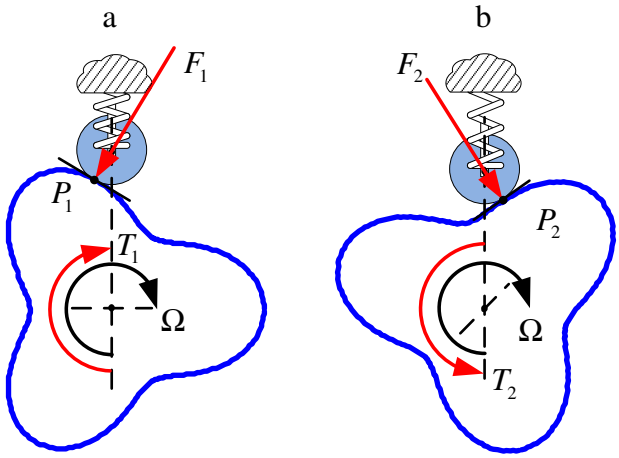

Fig. 2. Normal force exerted by a roller cam follower (F_1, F_2) and external torque exerted by the motor T_1 and T_2 on a cam rotating clockwise in a constant velocity Ω in two positions: (a) the pre-compressed elastic spring opposes rotation (F_1), while (b) the pre-compressed elastic spring aids rotation (F_2). Continuous contact between cam and follower is assumed at all times.

eight wavelengths ($M = 8$) with four cams per wavelength ($N_C = 32$), and three circumferential wavelengths per cam ($N = 3$). Schematics of the implemented robotic swimmer and a photograph of the waving mechanism are given in Figs. 2–3 and in Appendix A. The concept of operation of a single cam and its followers, and a wavelength set are animated in Clip 3 and Clip 4 respectively, using CAD (computer aided design) simulations.

2.1. Wave generator mechanism: kinematic analysis

To induce a traveling wave of a single wavelength, a pitch profile consisting of a single angular wavenumber should be designed. However, if a more complex wave is desired, one that requires several spatial harmonics, e.g. resembling a triangular or a square wave, the cam profile can be accordingly designed to comprise a sum of harmonic components. This profile can be represented by a Fourier series in terms of the spatial harmonics. A general pitch profile (Fig. 4) can be expressed in polar coordinates (r_p, θ) as

$$r_p = r_0 + \sum_{n=1}^{N_H} b_n \cos(nN\theta), \tag{1}$$

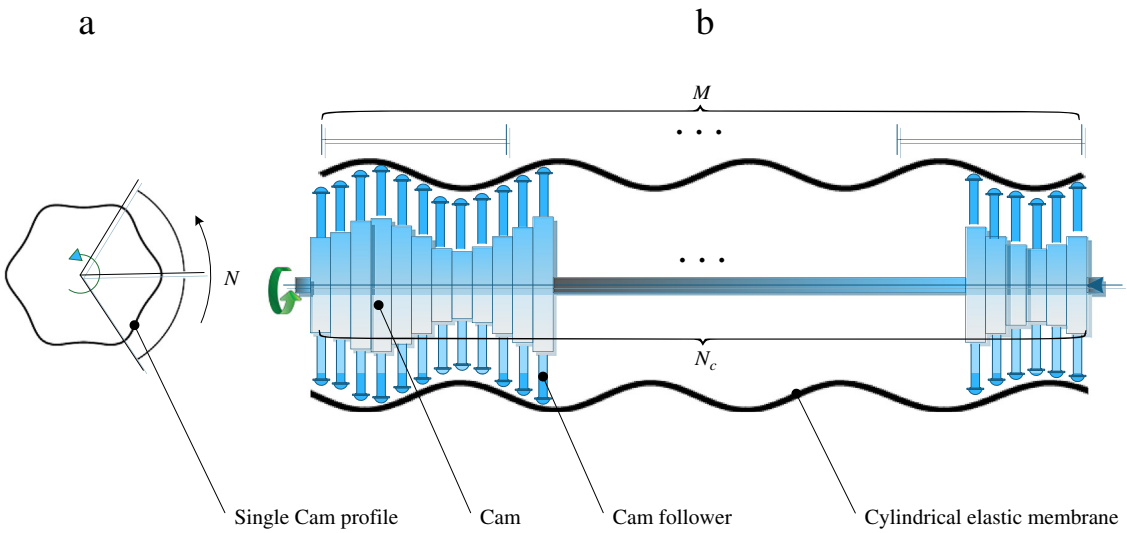

Fig. 3. Schematics of the wave generator mechanism: (a) front view of a typical single harmonic cam of six angular wavelengths ($N = 6$) and (b) side view of a cross-section of the waving mechanism. As the camshaft revolves, the radially translating cam-followers follow the rotating harmonic cams that are set along the camshaft in uniform angular phase to one another. The cam-followers push radially against the pre-tensioned cylindrical elastic membrane that is deforming in the desired tempo-spatial pattern, e.g. traveling waves.

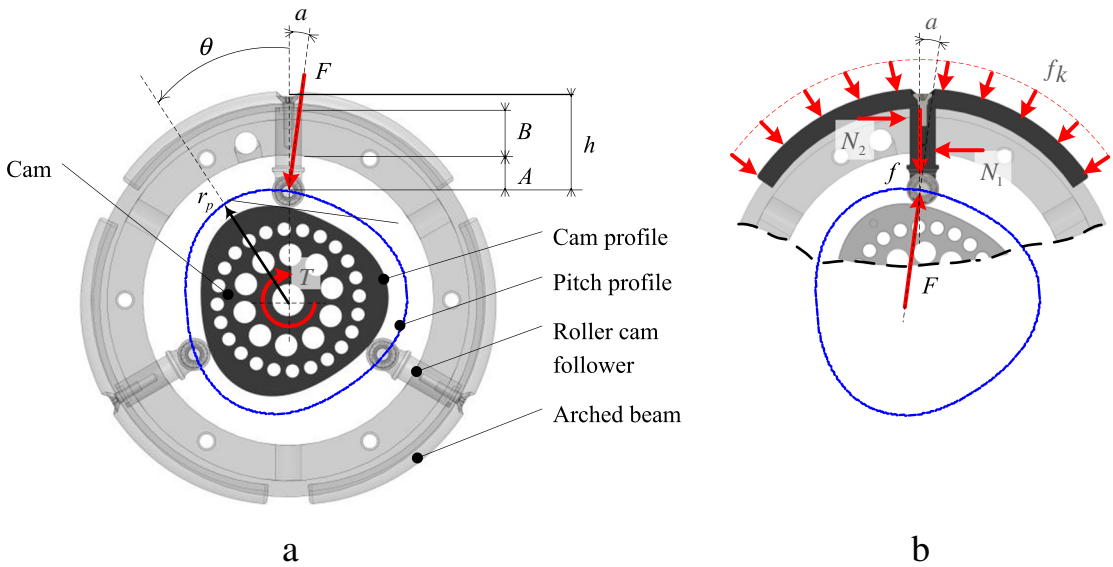

Fig. 4. Computer-generated image of (a) a cross-section of a harmonic cam with three roller followers. The pitch profile is composed of a single harmonic with three angular wavelengths ($N_H = 1$, $N = 3$). The normal force exerted by the cam follower F and the external torque by motor T are shown in red. (b) Forces acting on a cam follower (red): normal force due to cam contact F, normal forces due to linear bearing N_1, N_2, distributed elastic restoring forces due to cylindrical membrane f_k, and a general dissipative force f (roller follower rising).

where r_0 is the prime circle radius, N_H is the number of harmonics comprising the pitch profile, N is the number of angular wavelengths for the primary harmonic, $\theta = \Omega t$ is the angle of rotation, and b_n, $n = 1,\ldots,N_H$ are the amplitudes of each of the harmonics. It is further assumed that the cam-followers are of the roller type and the cam profile is designed to yield the desired pitch profile while compensating for the roller radius. Linear momentum balance on a cam follower (see for example Ref. [21,22]) results in the force exerted by a single roller follower on a cam, assuming a thin follower (direction of dry friction force is embedded in the sign of the sine term):

$$F = \frac{f_k + c\dot{r}_p + m_f\ddot{r}_p}{\cos\alpha - \mu\left(\frac{2A+B}{B}\right)\sin\alpha}, \tag{2}$$

where c is the viscous damping coefficient, μ is Coulomb friction coefficient, f_k is an elastic restoring force, α is the pressure angle, B is the length of the follower linear bearing, and A is the roller follower overhang (see Fig. 4).

Neglecting shell flexural rigidity compared with membranic effects [23] and assuming axial symmetry and small deflections of the elastic cylindrical membrane, it can be shown that the radial restoring force is linear and the radial stiffness is given by

$$k_S = EwS\left(\frac{d_0}{2}\right)^{-2} \tag{3}$$

where E is the elasticity modulus, w is the membrane thickness, S is a surface fraction covered by an arched beam, and d_0 is the undeformed diameter of the elastic cylindrical membrane. The elastic radial restoring force exerted by the cylindrical membrane is now given by

$$f_k = k_S\left(r_p + h - \frac{d_0}{2}\right) \tag{4}$$

where h is the follower length (Fig. 4). It is assumed at all times that the elastic cylindrical membrane maintains positive tension and provides enough restoring force to prevent cam-follower disengagements. Moreover, the cam follower overhang (Fig. 4) is given by

$$A = A_0 - (r_P - r_0), \tag{5}$$

where A_0 is the mean overhang. The pressure angle, the angle between the normal to the pitch curve and the follower velocity vector (see Fig. 4) is given by [22] (with zero follower offset)

$$\alpha = \tan^{-1}\left(\frac{1}{r_p}\frac{dr_p}{d\theta}\right), \tag{6}$$

(positive pressure angle where the follower is ascending, i.e. $dr_p/d\theta > 0$).

The torque exerted by a single cam-follower on a single cam is given by

$$T = r_p F \sin\alpha. \tag{7}$$

Substituting Eqs. (2)–(6) into Eq. (7) while exploiting cyclic symmetry of the design yields, after simplification, the torque exerted by N circumferential cam-followers on a single cam

$$T = \frac{N\left[k_s\left(r_p + h - \frac{d_0}{2}\right) + c\dot{r}_p + m_f r_p\right] r_p r'_p B}{r_p B - \mu\left[2\left(A_0 - r_p + r_0\right) + B\right] r'_p}, \tag{8}$$

where $r'_p \triangleq dr_p/d\theta$.

Since the torque load on each cam is periodic and since shaft torque oscillations should be eliminated, harmonic analysis of the torque is proposed. To this end let us denote

$$T = a_0 + \sum_{k=1}^{\infty} a_k \sin(kN\theta + \varphi_k), \tag{9}$$

where a_0 is the mean torque on a cam, a_k and φ_k are the amplitude and phase of the kth harmonic respectively in the torque signal.

It can be noticed from Eq. (8) that for the simple case where Coulomb friction is negligible ($\mu \to 0$), the torque on a cam is a linear combination of the terms r'_p, $r_p r'_p$, $\dot{r}_p r'_p$, and $r_p r'_p$. Assuming constant angular velocity (Ω) and relying on Eq. (1), the spatial (angular) frequencies of the torque contains energy at discrete, equally spaced spectral lines with respect to the rotation angle θ and are given by $\{(n \pm m)N\}$; $n,m = 0,1,2,\ldots N_H$. Moreover, the non-zero mean (DC) is contributed only by the term $\dot{r}_p r'_p$, which is preceded by the viscous damping coefficient. Furthermore, by averaging Eq. (8) over a period it can be shown that the mean torque on a single cam for negligible dry friction and non-negligible viscous damping, due to N circumferential cam-followers is given by

$$\langle T\rangle\Big|_{\substack{\mu = 0\\ c\neq 0}} = \frac{1}{2} c N^3 \Omega \sum_{n=1}^{N_H} n^2 a_n^2. \tag{10}$$

By assuming a pitch-profile of a single harmonic ($N_H = 1$) with a small amplitude a_1, expanding Eq. (8) in power series of the pitch radius amplitude a_1, and averaging over a period, it can be shown that the mean torque on a single cam is given by a series of even powers of the amplitude a_1. Even powers are expected since the mean non-zero torque due to friction cannot be affected by the mathematical sign of the amplitude, which is equivalent to shaft rotation. The leading order term of the mean torque (assuming small amplitude) is then given by

$$\langle T\rangle\Big|_{\substack{\mu\neq 0\\ c\neq 0\\ a_1 \ll 1}} \simeq \mu {a_1}^2 \frac{N^3 k_S}{2Br_0}(2A_0 + B)\left(r_0 + h - \frac{d_0}{2}\right) + \frac{1}{2} c {a_1}^2 N^3 \Omega. \tag{11}$$

The expression given in Eq. (11) is a sum of positive components, where $r_0 + h - d_0/2 > 0$ as it represents the mean radial displacement of the elastic cylindrical membrane, which is assumed to maintain positive tension all times. The expressions in Eqs. (10)–(11) are significant because, when multiplied by the number of cams N_C, they represent the optimal (minimal) resultant shaft torque in the presence of viscous damping and dry friction, respectively, where torque oscillations have been eliminated.

It follows that when both Coulomb friction and viscous damping are negligible, the torque on each cam oscillates with zero mean. However, when Coulomb friction is significant, its nonlinear contribution further increases the number of harmonics composing the periodic torque (Eq. (9)). In summary, the number of wavelengths in the desired wave N_H as well as the magnitude of the dry friction μ determine the number of harmonics comprising the periodic torque on a single cam.

The resultant torque on the camshaft from summing up the torques on each cam can be put as

$$T_t = \sum_{n=1}^{Nc} T(\theta)|_{\theta=\theta+(n-1)\Delta\theta} \tag{12}$$

where

$$\Delta\theta = 2\pi \frac{M}{NN_C} \tag{13}$$

is the uniform angular phase shift between successive cams along the camshaft to yield traveling waves. Substituting Eq. (9) into Eq. (12) yields after some manipulations

$$T_t = N_C a_0 + \Im\left[\sum_{k=1}^{\infty} a_k e^{i(\varphi_k + kN\theta)} \sum_{n=1}^{N_c} r^{n-1}\right], \quad r \triangleq e^{i\frac{2\pi kM}{N_C}}, \tag{14}$$

where $\Im[\ ]$ extracts the imaginary part of a complex number. The last representation is convenient in determining the optimal set of parameters that minimizes the torque oscillations, as described below.

2.2. Eliminating torque oscillations

As stated above, assuming $\mu = c = 0$ the mean torque is zero, i.e. $a_0 = 0$ in Eqs. (9) and (14). It is demonstrated below that the residual oscillating terms in the complex series in Eq. (14) equal zero individually for every k, provided that $k\,M$ is an integer number and kM/N_c is a non-integer for $k = 1, 2, 3,\ldots K$, where K is the highest harmonic of finite magnitude in Eq. (9).

Let us examine the complex geometric series

$$1 + r + r^2 + r^3 + \cdots + r^{N_c - 1} = \sum_{n=1}^{N_c} r^{n-1} = \frac{1 - r^{N_c}}{1 - r}, \quad r \triangleq e^{i\frac{2\pi kM}{N_C}}, \quad i \triangleq \sqrt{-1}. \tag{15}$$

From Eq. (15) it follows that

$$\sum_{n=1}^{N_C} e^{i(n-1)\frac{2\pi kM}{N_C}} = \frac{1 - e^{i2\pi kM}}{1 - e^{i\frac{2\pi kM}{N_C}}} = 0 \tag{16}$$

if

$$\frac{kM}{N_C} \notin \mathbb{Z}, \ kM \in \mathbb{Z}, \ k = 1, 2, \ldots, \tag{17}$$

where $\mathbb{Z}$ is the group of integer numbers. Substituting Eq. (16) into Eq. (14), while assuming Eq. (17) holds yields

$$T_t = N_C\, a_0. \tag{18}$$

For $\mu \neq 0$ or $c \neq 0$ it was shown that $a_0 \neq 0$, e.g. Eqs. (10)–(11). Hence, the mean total torque cannot be identically zero as its magnitude increases with the number of cams. However, its oscillation amplitude can be dramatically decreased by eliminating the harmonic sums in Eq. (14), provided that the assumptions made in Eq. (17) hold.

The last statement calls for optimization to find the optimal number of cams and wavelengths, given friction and damping parameters. Within the scope of this paper, an optimal torque results in a minimum cost function J that represents input power (i.e. ohmic or thermal losses in a DC motor) or minimal root mean square (RMS) over one shaft revolution (minimum signal energy):

$$\min_{M, N_C} J = \frac{1}{2\pi}\sqrt{\int_0^{2\pi} T_t^{\,2}(\theta)\, d\theta}. \tag{19}$$

This definition accounts for both mean magnitude and oscillation amplitude. Other optimization definitions may assign different weights to the mean torque or oscillation amplitude.

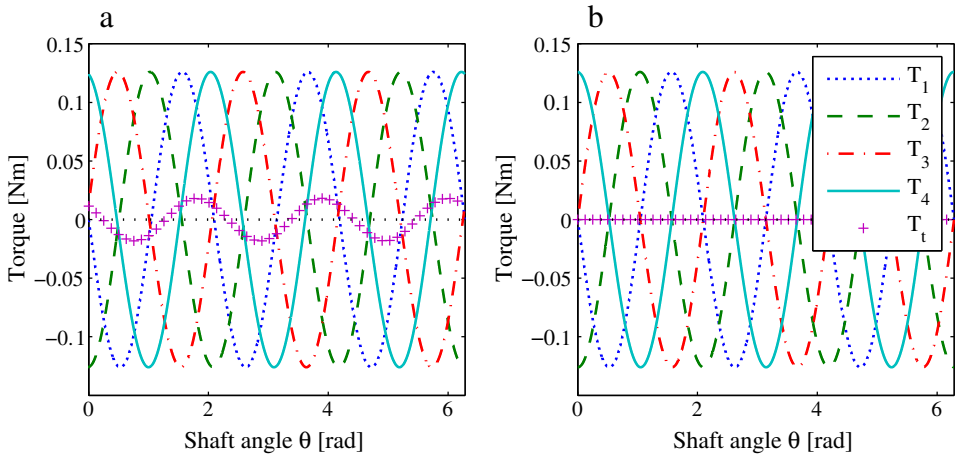

Fig. 5. Torque load curves on successive cams $T_1,\ldots,T_4$ and resultant torque T_t on the shaft vs. rotation angle for incorrect phase shift (a) where 1° error is deliberately introduced and (b) correct phase shift. Considerable torque oscillations result from a minor phase shift error. Curves are calculated assuming negligible dissipative losses ($\mu = c = 0$, $N = 3$, $N_C = 4$, $M = 1$).

3. Numerical examples

The effect of optimal angular phase-shift between the cams on the torque load on individual cams and on the resultant shaft torque is demonstrated in Figs. 4–5 for negligible and non-negligible dissipative losses, respectively. Choosing $N = 3$, $N_C = 4$ and $M = 1$, it can be easily derived from Eqs. (13) and (17) that $\Delta\theta = 30°$. It is shown in Fig. 5(a) that a slight deviation of one degree from the optimal relative angular rotation shift, i.e. non-optimal configuration, does not affect the torques on the individual cams T_i, $i = 1, 2, \ldots, N_C$ (it only introduces a phase shift). However, this small phase shift results in considerable resultant torque oscillations (purple pluses in Fig. 5). Clearly, the optimal phase shift between the cams that conforms to Eqs. (13) and (17) results in zero resultant shaft torque T_t, as depicted in Fig. 5(b).

When viscous damping is introduced, as depicted in Fig. 6, the non-optimal phase shift, given a phase error of one degree, results in significant total torque oscillations. An optimal relative phase can be produced that yields a non-zero constant torque without any torque oscillations. The mean torque cannot be eliminated since dissipation is not conservative and thus cannot be nullified by elastic forces. The magnitudes of the mean resultant shaft torque for viscous damping and for dry friction were successfully compared with the analytical expressions in Eqs. (10)–(11).

The effects of the frequency content of a single cam torque load signal on the cost function Eq. (19) are examined in Figs. 6–8 for various combinations of N_C and M values, provided that $N_C > 2$ and $N_C/M > 2$. Here, frequency content refers to spatial

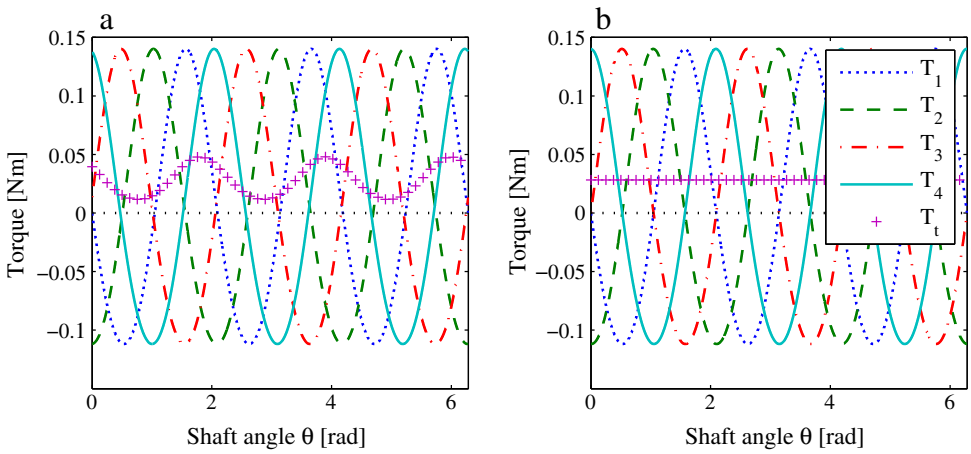

Fig. 6. Torque load curves on successive cams $T_1,\ldots,T_4$ and resultant torque T_t on the shaft vs. rotation angle for incorrect phase shift (a) where 1° error is deliberately introduced and (b) correct phase shift. Considerable torque oscillations result from a minor phase shift error. Curves are calculated assuming minor viscous damping that yields non-zero constant optimal resultant torque ($\mu = 0$, $c = 0.1$, $N = 3$, $N_C = 4$, $M = 1$).

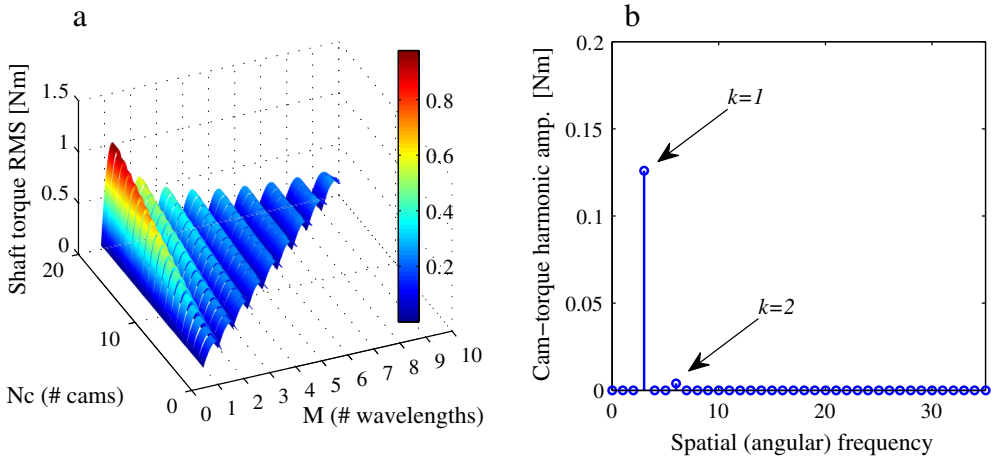

Fig. 7. (a) RMS of the shaft torque (Eq. (19)) plotted vs. number of cams and number of wavelengths in the mechanism, plotted for $\mu = c = 0$, $N = 3$, $N_H = 1$ $N_C > 2$, and $N_c/M > 2$. (b) Harmonic decomposition of the spatial (angular) frequencies of the torque on a single cam for $\mu = c = 0$, $N = 3$, $N_H = 1$. Where no dissipation is present the optimal shaft torque RMS can be set to zero, as appears here in the single harmonic cam ($N_H = 1$) along the lines of an integer number of wavelengths ($M \in \mathbb{Z}$).

(angular) frequencies that compose the torque on a single cam, i.e. the amplitudes a_k for each harmonic index $k = 0, 1, 2,...$ in Eq. (9).

As stated above, for a cam with a single harmonic profile ($N_H = 1$) and no dissipative losses, the torque signal is composed of only two harmonics with zero mean. Indeed Fig. 6(a) shows that the resultant shaft torque RMS is zero along the lines of $M \in \mathbb{Z}$ where the conditions in Eq. (17) are met, since $k = 1$ or 2 and $N_C > 2$. It can also be noted that the cam torque contains two harmonics and zero mean from the harmonic decomposition Fig. 6(b).

In the presence of dissipative losses, e.g. dry friction or viscous damping, the mean resultant shaft torque is always non-zero, since the dissipative forces are non-conservative and cannot be eliminated by any phase setting of the elastic restoring forces acting on the cams. Indeed it can be noted from Fig. 8(a), where viscous damping is introduced into the model ($c = 0.5$ $N\,s/mm$), that the optimal shaft torque RMS (minima area) is non-zero and increases with the number of cams, as predicted by Eq. (14). Moreover in Fig. 8(b) a non-zero component is present in the spatial frequency content.

As can be noted from Eq. (8), dry friction or a multi-harmonic cam-profile give rise to higher harmonics in the cam torque signal, which must be considered if the conditions in Eq. (17) are to be satisfied. In Fig. 9(a)–(b) the shaft torque RMS and the harmonic decomposition of the torque on a single cam are presented respectively for non-negligible friction and multi-harmonics cam profile ($\mu = 0.8$, $N_H = 7$). It is evident that higher harmonics are indeed present, which leads to non-trivial combinations for which $kM/N_C \in \mathbb{Z}$, thus violating the conditions in Eq. (17) that are required to guarantee no shaft torque oscillations. Indeed, it can

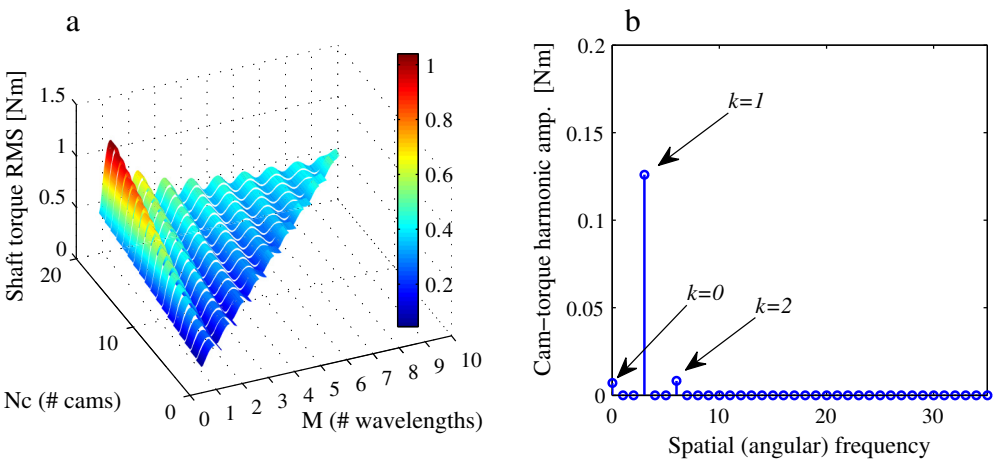

Fig. 8. (a) RMS of shaft torque (Eq. (19)) plotted vs. number of cams and number of wavelengths in the mechanism, plotted for $\mu = 0$, $c = 0.5 Ns/mm$, $N = 3$, $N_H = 1$, $N_C > 2$, and $N_c/M > 2$. (b) Harmonic decomposition of the spatial (angular) frequencies of the torque load on a single cam for $\mu = 0$, $c = 0.5 Ns/mm$, $N = 3$, $N_H = 1$. Dissipation results in non-zero mean cam torque and shaft torque. The shaft torque RMS increases with the number of cams.

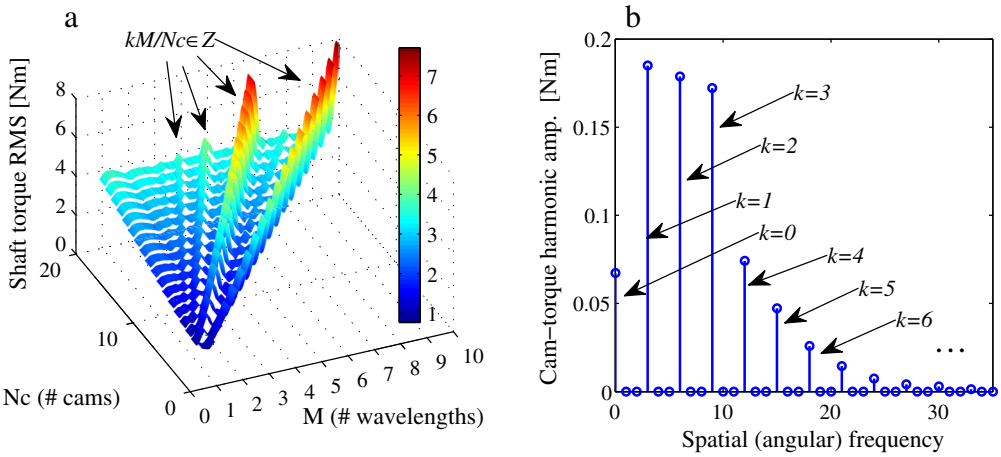

Fig. 9. (a) RMS of shaft torque (Eq. (19)) plotted vs. number of cams and number of wavelengths in the mechanism for $\mu = 0.8$, $N = 3$, $N_H = 7$, $N_C > 2$, and $N_c/M > 2$. (b) Harmonic decomposition of the spatial (angular) frequencies of the torque on a single cam for $N = 3$, $\mu = 0.8$, $N_H = 7$. Dry friction and cam profile of multi-harmonics ($N_H > 1$) give rise to higher harmonics in the cam torque, which results in torque oscillations as indicated by high RMS values, along the lines where $kM/M_C \in \mathbb{Z}, \quad k = 1, 2, 3, \ldots$.

be noted that considerable RMS magnitudes are found along the lines where $kM/N_C \in \mathbb{Z}$ in Fig. 9(a). In this more realistic case, an integer number of wavelengths ($M \in \mathbb{Z}$) is definitely not sufficient to obtain no torque oscillations, and more careful attention is required in the design.

4. Proposed applications

As discussed above, the proposed mechanism can be utilized to drive traveling surface waves for means of fluid manipulations, i.e. perform as a pump or a free swimmer in low Reynolds environments that are common in extremely viscous fluids or in micro scales.

A pump can be realized in a manner similar to that depicted in Fig. 10. In this configuration, the waving mechanism is placed inside a pipe filled with fluid. As the waves propagate along the mechanism, the fluid that is trapped between the waving surface and the pipe wall is pushed forward in the direction of the wave propagation. Since this type of pump does not involve any rotating or mating parts that are in contact with the fluid, it allows a low shearing rate, which makes it favorable in conveying shear sensitive particles or molecules as in biological applications.

If the pump was released from its fixations, it would perform as a swimmer. Indeed, a robotic swimmer was designed, fabricated and tested in highly viscous silicone fluid (60,000 cSt). The robotic swimmer (50 cm long 60 mm wide) is depicted in Fig. 11. The swimmer is wireless and is propelled by the proposed waving mechanism. The swimmer includes on-board power source (batteries) and microprocessor that generates controlled PWM (pulse width modulation) signals to drive a DC motor that rotates the camshaft (Appendix A). The desired speed and direction commands are transmitted from a remote computer using Bluetooth™ communication. The swimmer transmits back the motor speed (magnetic encoder) and swimmer orientation (static accelerometers). The position of the swimmer is traced by a video camera. Experimental investigation of the effects of wavelength and wave velocity on the swimming speed and comparison with an analytical model is given in Ref. [18]. The waving surface of the experimental robotic swimmer is shown in Clip 1 and a zoomed out view of free swimming is given in Clip 2.

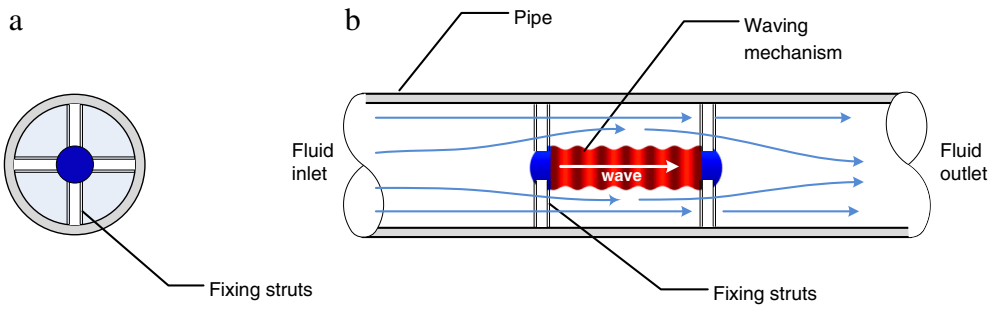

Fig. 10. Front view (a) and side view (b) of a schematic illustration of a proposed realization of an inline pump for viscous fluids using the described waving mechanism. The pump is installed in the center of a pipe by fixing struts. The fluid trapped in the circumferential gap between the waving mechanism and the pipe wall is forced to move in the direction of the wave propagation.

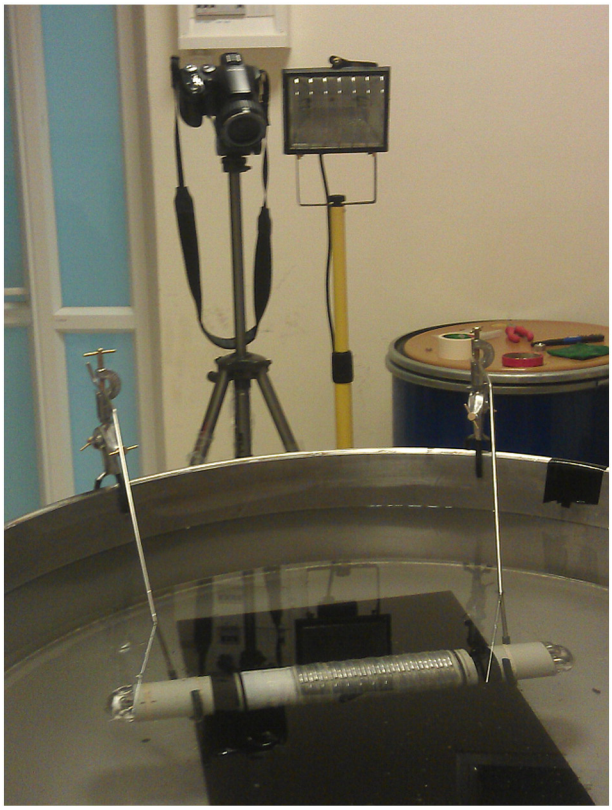

Fig. 11. An image of the experimental robotic swimmer employing the proposed mechanism. The swimmer is placed in a tank of silicone fluid (kinematic viscosity of 60.000 cSt) tracked by a video camera. The swimmer in the image is held fix to capture better the waving surface. In the swimming experiment, the fixtures are removed and the swimmer is free to propagate (in the direction opposite to the direction of wave propagation).

5. Conclusions

A multi-cam mechanism that generates traveling waves along a cylindrical elastic membrane as a means for propulsion/pumping was analyzed, designed and fabricated. Analytical and numerical demonstrations showed that an optimized angular shift between successive cams can be found in order to ensure minimal internal input torque. A constant non-oscillating resultant shaft torque is obtained if the number of wavelengths times spatial frequency index is an integer ($kM \in \mathbb{Z},\ k = 1, 2, 3, \ldots$) and the last multiplication over the number of cams is a non-integer $kM/N_C \notin \mathbb{Z}$. The second condition is important when the torque on a single cam is composed of several spatial (angular) frequencies, as in the case of multi-harmonic cam profile or when dry friction cannot be ignored. It was demonstrated that for a cam of single harmonic profile, assuming no dissipation, the torque signal is composed of only two harmonics with zero mean. Thus the resultant shaft torque can be set to zero. In this configuration the circumferential elastic cylindrical membrane deforms as a traveling wave, thus remaining in a state of equi-elastic-potential surface. The optimal resultant shaft torque in the case where dissipative losses, e.g. dry friction or viscous damping, are present is a non-zero constant. Where dissipation cannot be ignored, it was found that the optimal residual mean torque is proportional to the damping or friction magnitude, proportional to the pitch profile amplitude squared, and proportional to the number of circumferential wavelengths cubed. In the case of viscous damping the residual torque is also proportional to the angular velocity of rotation, and in the case of dry friction the residual torque is proportional to the mean restoring elastic force.

Numerical examples demonstrated the validity of the required conditions for eliminating shaft torque oscillations with respect to spatial frequency content of torque signals. Moreover, the numerically calculated magnitudes of the mean shaft torque where dissipation losses are present were compared successfully to the analytical model and approximation.

A prototype robot applying the proposed waving mechanism was designed, fabricated and tested successfully as a swimmer in viscous fluid.

Supplementary data to this article can be found online at http://dx.doi.org/10.1016/j.mechmachtheory.2013.07.017.

Acknowledgments

The authors wish to acknowledge Mr. Amir Setter, Dr. Harel Plat, and Mr. Nadav Cohen, for fruitful discussions.

Appendix A. Implementation of the proposed mechanism: A robotic swimmer

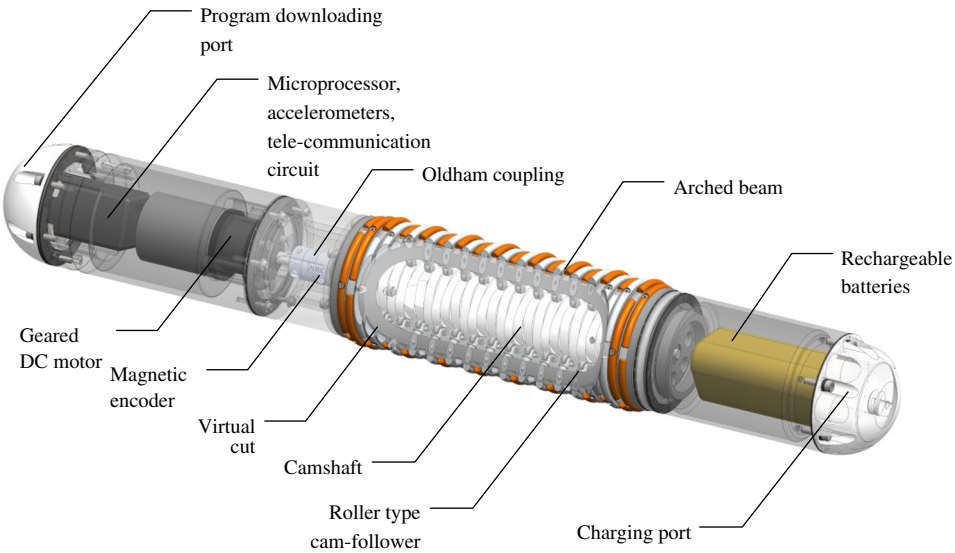

Fig. 12. CAD model of the robotic swimmer that utilizes the wave-generator mechanism. The robotic swimmer is designed for natural buoyancy and levelness when immersed in silicone fluid (density of 967 kg/m^3).

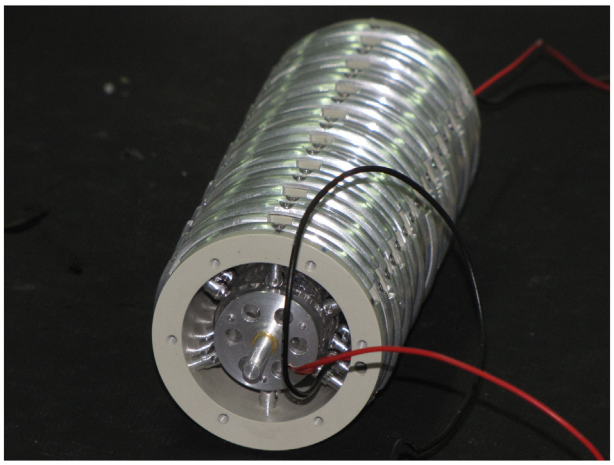

Fig. 13. A photograph of the waving mechanism section of the robotic swimmer before encapsulation in the elastic cylindrical membrane. Camshaft and cam-followers are visible inside the polypropylene cylinder that performs as linear bearings for the cam-followers. Aluminum arched beams bolted to the cam-followers are visible at the outer circumference.

References

[1] R. Gabai, I. Bucher, Excitation and sensing of multiple vibrating traveling waves in one-dimensional structures, Journal of Sound and Vibration 319 (1–2) (2009) 406–425.
[2] S. Ueha, Y. Tomikawa, Ultrasonic Motors: Theory and Applications, with Contributions from M. Kurosawa and N. Nakamura, Clarendon Press, Oxford, 1993.
[3] M. Jean-François, B. Stéphane, B. François, On the generation and identification of traveling waves in non-circular structures — application to innovative piezoelectric motors, Smart Materials and Structures 7 (3) (1998) 337.
[4] A. Minikes, I. Bucher, Noncontacting lateral transportation using gas squeeze film generated by flexural traveling waves — numerical analysis, Journal of the Acoustical Society of America 113 (5) (May 2003) 2464–2473.
[5] L. Chen, S. Ma, Y. Wang, et al., Design and modelling of a snake robot in traveling wave locomotion, Mechanism and Machine Theory 42 (12) (2007) 1632–1642.
[6] C. Li, W. Yuechao, M. Shugen, et al., Analysis of traveling wave locomotion of snake robot, Robotics, Intelligent Systems and Signal Processing, Proceedings. IEEE International Conference on, vol. 1, IEEE, 2003, pp. 365–369.
[7] B. Chan, N.J. Balmforth, A.E. Hosoi, Building a better snail: lubrication and adhesive locomotion, Physics of Fluids 17 (11) (Nov. 2005).
[8] K.H. Low, Modelling and parametric study of modular undulating fin rays for fish robots, Mechanism and Machine Theory 44 (3) (2009) 615–632.

[9] S. Childress, Mechanics of Swimming and Flying, 1981.
[10] N. Cohen, J.H. Boyle, Swimming at low Reynolds number: a beginners guide to undulatory locomotion, Contemporary Physics 51 (2) (2010) 103–123, (2010/03/01).
[11] C. Brennen, H. Winet, Fluid mechanics of propulsion by cilia and flagella, Annual Review of Fluid Mechanics 9 (1) (1977) 339–398.
[12] J.J. Abbott, K.E. Peyer, M.C. Lagomarsino, et al., How should microrobots swim? International Journal of Robotics Research 28 (11-12) (2009) 1434–1447, (November/December 2009).
[13] A.H. Meng, N.-T. Nguyen, R.M. White, Focused flow micropump using ultrasonic flexural plate waves, Biomedical Microdevices 2 (3) (2000) 169–174.
[14] K. Nakahara, K. Yoshimura, Y. Okayama, et al., A peristaltic micropump using traveling waves of polymer membranes driven by a single actuator, Micro Electro Mechanical Systems (MEMS), IEEE 24th International Conference on, 2011, pp. 1083–1086.
[15] B.J. Nelson, I.K. Kaliakatsos, J.J. Abbott, Microrobots for minimally invasive medicine, Annual Review of Biomedical Engineering 12 (1) (2010) 55–85, (2010/07/01).
[16] E. Setter, I. Bucher, Flexural vibration patterning using an array of actuators, Journal of Sound and Vibration 330 (6) (2011) 1121–1140.
[17] M.P. Norton, Fundamentals of Noise and Vibration Analysis for Engineers, Cambridge University Press, 1989.
[18] E. Setter, I. Bucher, S. Haber, Low-Reynolds-number swimmer utilizing surface traveling waves: analytical and experimental study, Physical Review E 85 (6) (2012) 066304.
[19] E. Lauga, T.R. Powers, The hydrodynamics of swimming microorganisms, Reports on Progress in Physics 72 (9) (Sep. 2009) 36.
[20] G. Taylor, Analysis of the swimming of microscopic organisms, Proceedings of the Royal Society of London. Series A: Mathematical and Physical Sciences 209 (1099) (Nov. 22, 1951) 447–461.
[21] H.A. Rothbart, Cam Design Handbook, McGraw-Hill, 2004.
[22] J.K. Mills, L. Notash, R.G. Fenton, Optimal design and sensitivity analysis of flexible cam mechanisms, Mechanism and Machine Theory 28 (4) (1993) 563–581.
[23] S. Timoshenko, S. Woinowsky-Krieger, Theory of Plates and Shells (Engineering Societies Monographs), 2nd ed. McGraw-Hill, 1959.